Received: 27 June 2023 | Revised: 2 August 2023 | Accepted: 20 August 2023

DOI: 10.1002/app.54655

RESEARCH ARTICLE

Applied Polymer Science WILEY

Interplay of curing and thermal degradation in epoxy resins cured with amino acids: Influence of the maximum curing temperature on the network structure, crystal morphology and mechanical properties

Florian Rothenhäusler | **Holger Ruckdaeschel**

Department of Polymer Engineering, University of Bayreuth, Bayreuth, Germany

Correspondence
Holger Ruckdaeschel, Department of Polymer Engineering, University of Bayreuth, Universitätsstraße 30, 95447 Bayreuth, Germany.
Email: holger.ruckdaeschel@uni-bayreuth.de

Funding information
German Federal Ministry for Economic Affairs and Climate Action (BMWK), Grant/Award Number: 20E1907A

Abstract

Bio-based alternatives for epoxy resin curing agents are a necessity for fiber reinforced polymer composites to become more sustainable. Here, the precise knowledge about the optimal curing cycle and its influence on the thermoset's mechanical properties are imperative. Therefore, the influence of the maximum curing temperature on the network structure, crystal morphology and mechanical properties of diglycidyl ether of bisphenol A (DGEBA) cured with L-arginine was investigated with the goal to derive structure–property relationships and a favorable curing cycle. The maximum curing temperature used can be categorized into two regimes: first, the temperature range in which the thermoset reaches complete curing and second, the temperature regime in which the thermoset is fully cured and the thermal degradation starts to diminish its mechanical properties. An optimized curing regimen for achieving high flexural strength accompanied by adequate fracture toughness entails subjecting the material to a curing cycle comprising a duration of 1 h at a temperature of 150°C, followed by an additional 2 h at a temperature of 170°C. This study represents a pioneering effort in optimizing the curing process of amino acid-cured epoxy resin, specifically focusing on achieving the most favorable mechanical properties as a result.

KEYWORDS

amino acid, bio-based, curing cycle, epoxy resin, mechanical properties, network structure, thermal degradation

1 | INTRODUCTION

Epoxy-based thermosets play a crucial role in the field of fiber reinforced composites for various applications such as sports, automotive, and aerospace industries.[1,2] The crucial factors contributing to their importance include the high glass transition temperature, modulus, strength, and low viscosity of epoxy resins.[3] To address the growing demand for sustainable alternatives in fiber-reinforced composites, extensive research has been conducted in recent

decades on bio-based epoxy resins, curing agents, and natural fibers.[4,5] In recent years, there has been increasing interest in using amino acids as bio-based, latent curing agents for epoxy resins.[6–12] These amino acid-based thermosets have demonstrated performance levels comparable to conventional matrix materials used in fiber reinforced composites.[13,14] While previous studies have investigated the curing kinetics of epoxy resins with amino acids using differential scanning calorimetry (DSC), none have established an appropriate temperature–time profile for curing epoxy resins with amino acids in combination with commonly used accelerators.[7–9,11]

Insufficient curing periods and/ or curing temperatures lead to an incomplete curing of the thermoset.[15–17] A low degree of cure α leads to a decreased cross-link density ν_C which in turn results in a decreased modulus E and glass transition temperature T_g.[14,18–20] However, a decreased cross-link density correlates positively with an increased critical stress intensity factor K_{IC} and fracture energy G_{IC}.[21]

In contrast, when exposed to elevated temperatures in a standard atmosphere, the network structure of thermosets undergoes thermal-oxidative aging.[22] This aging process can be categorized into physical aging and chemical aging, each leading to distinct changes in the network structure. Physical aging occurs due to the relaxation of the thermoset network, resulting in alterations in the glass transition temperature and modulus.[23–25] On the other hand, chemical aging refers to changes in the network caused by chemical reactions such as post-curing, formation of carbonyl groups, and chain scission. These reactions can cause the thermoset to darken in appearance and experience a decline in its mechanical properties.[26–29] Consequently, it is crucial to carefully design curing cycles that ensure complete curing while mitigating the risk of thermal-oxidative aging. Although there is a wealth of literature concerning the thermal stability and decomposition processes of amino acid solutions or pure amino acids,[30–32] a notable gap exists in understanding their thermal stability as curing agents in epoxy resin and potential chemical reactions at elevated temperatures during the curing process of thermosets. This area remains largely unexplored in current research.

The investigation of these topics holds particular significance in the context of amino acid-cured epoxy resins, primarily due to the tendency of amino acids to form crystals during the thermoset curing process. This phenomenon has been observed in the curing of DGEBA with L-tyrosine, where the amino acid crystals act as reinforcement and contribute to the toughening of the epoxy matrix.[33] In general, amino acids exhibit lower thermal stability compared to epoxy resin-based thermosets in which they are embedded.[34–36] The thermal stability of amino acid crystals is heavily influenced by the structure of the amino acid's side chain.[36] For instance, the decomposition temperature of the aromatic amino acid L-tyrosine is approximately 340°C,[37,38] while the thermal degradation of the aliphatic amino acid L-glutamine initiates at around 185°C.[36]

The thermal degradation or decomposition of amino acids involves several reactions: the peptide reaction, decarboxylation, and deamination.[31] In the peptide reaction, the hydroxyl group of the carboxylic acid in one amino acid reacts with a hydrogen atom from the amino group of another amino acid, resulting in the formation of water.[39,40] Consequently, the network structure of amino acid-cured epoxy resins can contain not only bonds between the epoxy resin and the amino acid curing agents but also bonds between the amino acids themselves.[41] This reaction has been observed in amino acids such as L-histidine, L-arginine, and L-aspartic acid during thermal degradation. Deamination is a condensation reaction that involves the formation of ammonia through the condensation of an amino group with a hydrogen atom.[42] This reaction has been observed in amino acids such as L-glutamine, L-glycine, and L-arginine.[36] Both reactions result in the formation of volatile compounds with low molecular weight, namely water and ammonia. As a result, amino acids experience a loss of mass and volume during thermal degradation, leading to shrinkage of amino acid crystals and changes in their crystal structure and morphology. Additionally, the formation of cyclic peptides or bicyclic peptides may occur.[36] Figure 1 illustrates the initial step in the thermal degradation of L-arginine, where the amino acid releases ammonia and

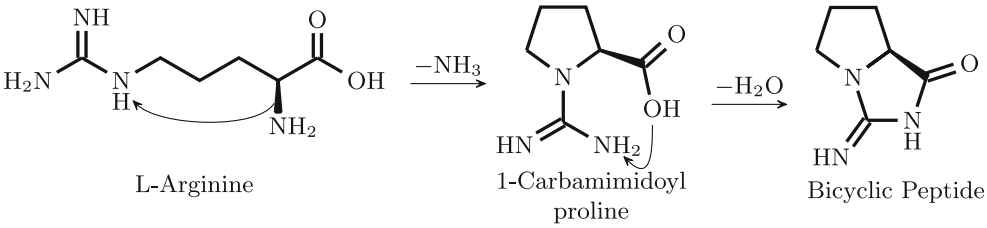

FIGURE 1 Condensation reaction of L-arginine by which the cyclic compound 1-carbamimidoylproline is formed and ammonia is released. Peptide reaction that changes the cyclic 1-carbamimidoylproline to a bicyclic peptide.

transforms into 1-carbamimidoylproline. Subsequently, the peptide reaction can lead to the formation of a bicyclic peptide with either the =NH or NH_2 group.

The objective of this investigation is to examine the influence of the maximum curing temperature on the thermal degradation, degree of cure, network structure, and mechanical properties of an epoxy resin cured with an amino acid. To achieve this, a systematic approach is proposed: First, thermal degradation of the amino acid: Thermo-gravimetric analysis (TGA) and Fourier-transform infrared spectroscopy (FTIR) will be conducted to investigate the thermal degradation of the amino acid itself. These techniques will provide insights into the amino acid's degradation mechanism and chemical changes occurring during the curing process. Second, analysis of cured thermosets: The epoxy resin cured with various curing cycles at different maximum temperatures will be analyzed using FTIR, TGA, DSC, and mechanical testing. FTIR will assess the degree of thermal degradation and examine the chemical changes in the thermoset. TGA will provide information about the thermal stability of the cured thermosets and assess the degree of thermal degradation. DSC will analyze the degree of cure and thermal behavior, while mechanical testing (such as dynamic mechanical analysis (DMA), three-point bending and compact tension tests) will evaluate the mechanical properties. Lastly, correlation of results: The results obtained from DSC and mechanical testing will be correlated with each other to gain a comprehensive understanding of the interdependencies between network characteristics and mechanical properties. This analysis will provide insights into the relationship between curing parameters, network structure, and resulting mechanical performance. The ultimate goal is to identify an optimal curing cycle that achieves fast and complete curing without compromising the thermoset's integrity due to degradation. The chosen material system for this investigation involves DGEBA and L-arginine, as it has been extensively studied in previous research.[12,13]

2 | EXPERIMENTAL

2.1 | Materials

DGEBA resin, specifically D.E.R. 331, with an epoxide equivalent weight of 187 g mol^{-1} was utilized in this study. It was obtained from Blue Cube Assets GmbH & Co. KG, Olin Epoxy (Stade, Germany). L-Arginine, with a purity of 98.9%, was procured from Buxtrade GmbH (Buxtehude, Germany). The reaction between the amino acid and epoxy resin was facilitated by the use of the substituted urea DYHARD®UR400, provided by Alzchem Group AG (Trostberg, Germany).

2.2 | Resin formulation

The amino acid and epoxy resin mixture was prepared using a three-roll milling process, following the settings described in Reference 12. Based on previous investigations,[10,12,13] it was assumed that L-arginine has seven active hydrogen atoms ($f = 7$), resulting in an amine equivalent weight of 24.89 g mol^{-1}. The mixture of DGEBA and amino acid was formulated to achieve a stoichiometric ratio of active hydrogen atoms to epoxy groups ($R = 1$). Prior to mixing, one weight percentage of DYHARD®UR400 (refer to Table 1) was added. The mixing process was performed using a DAC 150.1 FVZ centrifuge speed mixer from Hauschild Engineering (Hamm, Germany) operating at 3000 min^{-1} for 120 s. Subsequently, the mixture was subjected to degassing for 30 min at 10 mbar to remove any entrapped air before the curing process. Throughout this investigation, the cured thermoset material is referred to as "Argopox" for simplicity.

2.3 | Curing cycle and sample preparation

The amino acid-epoxy mixture was carefully poured into pre-heated aluminum molds, which were maintained at a temperature of 90°C. The curing process took place in a Memmert ULE 400 convection oven, manufactured by Memmert GmbH + Co. KG (Schwabach, Germany). The curing cycle involved two steps. Initially, the thermoset was cured for 1 h at a constant temperature of 150°C. Subsequently, it underwent a second curing step for 2 h at temperatures ranging from 150 to 200°C, increasing in steps of 10°C (refer to Figure 2).

Due to the varying maximum temperature in each curing cycle, the thermosets were labeled as A150, A160, and so on, indicating the maximum temperature reached during their respective curing processes. To prevent the development of internal stresses, the molds were allowed to cool down to room temperature over a period of approximately 2 h. Specimens for testing were prepared using a Mutronic DIADISC5200 diamond plate saw, provided by MUTRONIC Präzisionsgerätebau GmbH & Co. KG

TABLE 1 Composition of Argopox.

Component	Argopox (wt%)
D.E.R. 331	87.4
L-Arginine	11.6
DYHARD®UR400	1

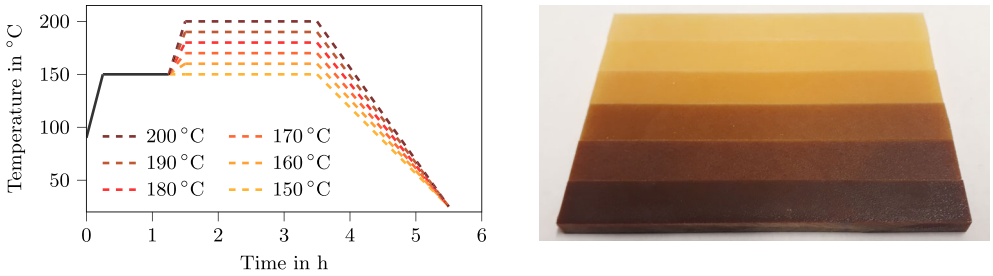

FIGURE 2 Left: Curing cycles employed for the preparation of Argopox with maximum curing temperatures from 150 to 200°C in steps of 10°C. Right: Overview about Argopox after different curing cycles. The thermosets are arranged low (A150, top) to high curing temperatures (A200, bottom). [Color figure can be viewed at wileyonlinelibrary.com]

(Rieden am Forggensee, Germany) in accordance with the relevant test method standards.

2.4 | Material characterization

2.4.1 | Thermo-gravimetric Fourier-transform infrared spectroscopy

Thermo-gravimetric Fourier-transform infrared spectroscopy was carried out by combining a Mettler Toledo TGA/SDTA 851E from Mettler-Toledo International Inc. (Columbus, OH) with a Nicolet iS50 FTIR spectrometer from Thermo Fisher Scientific Inc. (Waltham, MA). The sample was heated from 25 to 250°C with a constant heating rate of 2°C min^{-1} in a nitrogen atmosphere. The volatile degradation products were analyzed every 30 s by averaging 32 scans in a wavenumber-range from 500 to 4000 cm^{-1} in transmission mode.

2.4.2 | Thermo-gravimetric analysis

The thermo-gravimetric analyses were conducted on a Netzsch 209 F1 Libra from Erich Netzsch GmbH & Co. Holding KG (Selb, Germany). Here, the pure L-arginine was subjected to the curing cycles depicted in Figure 2 in synthetic air. The cured thermosets (Argopox) were heated from 25 to 600°C with a constant heating rate of 1°C min^{-1} in a nitrogen atmosphere.

2.4.3 | Fourier-transform infrared spectroscopy

Fourier-transform infrared spectroscopy (FTIR) was carried out using a Nicolet iS50 FTIR spectrometer from Thermo Fisher Scientific Inc. (Waltham, MA). Thirty-two scans per sample were averaged in a wavenumber-range from 500 to 4000 cm^{-1} in transmission mode.

2.4.4 | Differential scanning calorimetry

The degree of cure α and the glass transition temperature T_g of Argopox after the different curing cycles were determined with dynamic DSC measurements. A Mettler Toledo DSC 1 (Columbus, OH) was employed with a heating rate of 10 K min^{-1} from 25 to 275°C. Here, the flow of nitrogen was set to 50 mL min^{-1}. The sample mass was 20 ± 2 mg. Two specimens per curing cycle were tested. The degree of cure α was calculated as:

$$\alpha_x = \frac{H_0 - H_x}{H_0}, \tag{1}$$

with the heat of reaction H_0 of the uncured compound and H_x the remaining enthalpy after curing at x°C. The heat of reaction H_0 was determined to be 282.6 J g^{-1}.

2.4.5 | Dynamic mechanical analysis

Dynamic mechanical analysis (DMA) was performed using a Gabo Eplexor 500 N instrument from Gabo Qualimeter Testanlagen GmbH (Ahlden, Germany) in tension mode. The specimens, measuring 50 mm by 10 mm by 2 mm, were subjected to measurements from 25 to 180°C at a constant heating rate of 3 K min^{-1}. The tensile force amplitude was set to 60 with a frequency of 1 Hz. The glass transition temperature T_g was determined as the temperature at which the loss factor tan δ reaches its peak value. To calculate the cross-link density ν_C of the thermoset, the storage modulus E' at $T = T_g + 50$ K was used in the following equation:

$$\nu_C = \frac{E'}{3RT}, \tag{2}$$

where, R is the universal gas constant (8.314 J mol^{-1} K^{-1}).[20] To ensure accuracy, three specimens were tested for each curing cycle. The exact

dimensions of each specimen were determined with a caliper with a precision of ±0.01 mm.

2.4.6 | Three-point bending

For the three-point bending tests, a total of eight specimens were prepared for each thermoset. The specimens had dimensions of 80 mm by 10 mm by 4 mm. The bending tests were conducted using a ZwickRoell Z2.5 universal testing machine, manufactured by ZwickRoell GmbH & Co. KG (Ulm, Germany). The tests were carried out with a cross-head speed of 2 mm min^{-1}, following the guidelines specified in ISO 178. The exact dimensions of each specimen were determined with a caliper with a precision of ±0.01 mm.

2.4.7 | Fracture toughness

The critical stress intensity factor in mode I, denoted as K_{IC}, and the fracture energy, represented as G_{IC}, were evaluated by conducting tests on eight compact tension specimens per curing cycle. The testing was performed in accordance with ISO 13586 standards. A ZwickRoell Z2.5 testing machine, manufactured by ZwickRoell GmbH & Co. KG (Ulm, Germany), equipped with a load cell having a capacity of 2.5 kN, was utilized for these tests.

2.4.8 | Scanning electron microscopy

The fracture surfaces of the compact tension specimens were analyzed using a Zeiss Gemini 1530 Scanning Electron Microscope (SEM) manufactured by Carl Zeiss AG in Oberkochen, Germany. For the SEM imaging, an acceleration voltage of 3 kV was utilized. Prior to imaging, the surfaces of the specimens were coated with a thin layer of platinum through a process known as platinum sputtering, resulting in a coating thickness of approximately 5 nm.

3 | RESULTS AND DISCUSSION

3.1 | Thermo-gravimetric Fourier-transform infrared spectroscopy of L-arginine

To investigate the thermal degradation mechanism of L-arginine, thermo-gravimetric analysis coupled with Fourier-transform infrared spectroscopy is performed in a nitrogen atmosphere. The TGA curve of L-arginine in a nitrogen atmosphere, shown in Figure 3, reveals important features. Initially, between temperatures of 25 and 75°C, there is a mass loss attributed to the evaporation of water from the amino acid. After the drying process, the mass remains nearly constant until approximately 205°C. Beyond this temperature, the degradation mechanisms depicted in Figure 1 come into play. The amino acid undergoes a transformation to 1-carbamimidoylproline through the release of ammonia, followed by the formation of a bicyclic peptide via the condensation of water during the peptide reaction.[36] The FTIR analysis in Figure 3 confirms the presence of the reaction products. The twin peaks centered around 950 cm^{-1} correspond to ammonia,[43] while the peaks around 1700 and 3300 cm^{-1} are indicative of water.[44]

However, this dynamic measurement does not reflect the true temperature regimes that the epoxy resin system

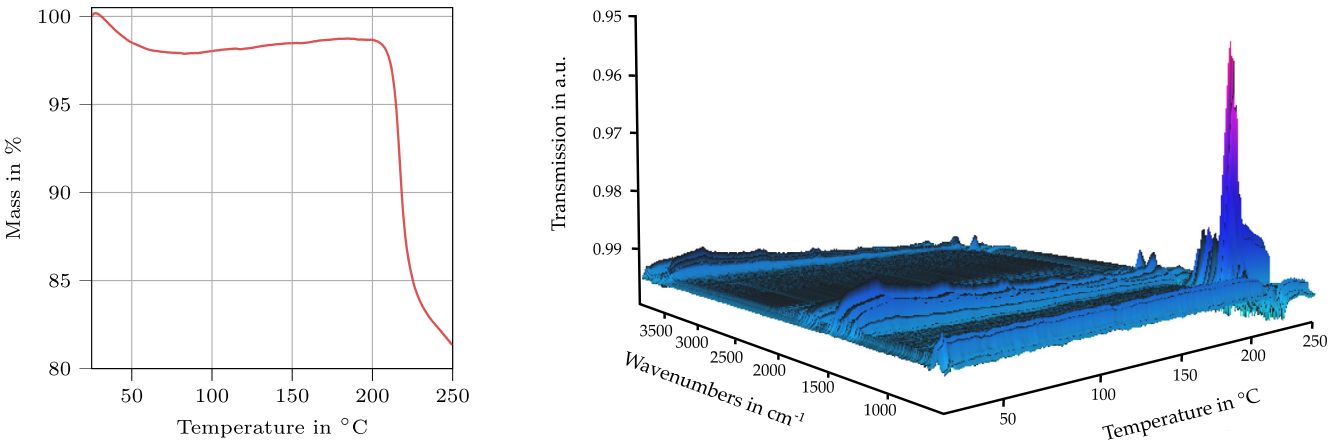

FIGURE 3 Left: Thermo-gravimetric analysis of L-arginine. Right: FTIR analysis of volatile degradation products during the thermo-gravimetric analysis of L-arginine. [Color figure can be viewed at wileyonlinelibrary.com]

undergoes during curing. It is essential to investigate the effect of the different curing cycles on L-arginine. Therefore, iso-thermal TGA measurements in synthetic air that mimic the curing cycles of the epoxy resin system (see Figure 2) are conducted (see Figure 4). After the temperature increase from 25°C, the specimens are initially held at 150°C for 60 min, during which no significant mass loss is observed. Subsequently, the temperature is increased to the respective maximum curing temperature for a duration of 2 h. At temperatures between 150 and 170°C, no significant thermal degradation occurs in L-arginine. However, at 180°C, a slight mass loss of approximately 1% is observed after an extended period. A temperature of 190°C initiates thermal degradation after approximately 10 min, resulting in a mass loss of about 15.5% after 2 h. At 200°C, the thermal degradation commences immediately, with a steep drop in mass followed by a flattening of the curve. The observed 20% mass loss can be explained by considering the molecular masses of L-arginine (174.2 $g\,mol^{-1}$), ammonia (17 $g\,mol^{-1}$), and water (18 $g\,mol^{-1}$). The combined molecular mass of ammonia and water is approximately 35 $g\,mol^{-1}$, accounting for about 20% of 174.2 $g\,mol^{-1}$. Overall, these findings provide insights into the thermal degradation behavior of L-arginine and its implications for the curing process of the epoxy resin system.

3.2 | Thermo-gravimetric analysis of Argopox

In order to gain insight into the thermal degradation of the Argopox thermoset, thermo-gravimetric analysis is performed on specimens cured at different maximum temperatures T_{max}. The objective is to examine how the degradation mechanism observed in pure L-arginine translates to the L-arginine crystals present in the thermoset. Figure 5 reveals two significant observations that support the assumption of a correlation between the thermal degradation mechanisms of pure L-arginine and the L-arginine crystals in the thermoset. First, increasing T_{max} results in a reduction of mass loss that occurs around 205°C. This indicates that the amino acid crystals in A150 and A160 remain undegraded during curing, and the observed mass loss can be attributed to the reactions discussed in Section 3.1. On the other hand, A200 shows no steep mass loss at this temperature, indicating that the crystals have already undergone the chemical changes associated with the thermal degradation at around 200°C.

These findings align with the results presented in Figure 4, further supporting the notion that the degradation mechanisms observed in pure L-arginine are indeed present in the thermoset. Second, the residual mass at 600°C increases from A150 to A200, with values of 12.0% and 13.5%, respectively. This difference in residual mass reflects the varying degrees of degradation that have already taken place during the curing process of the thermosets. Taken together, these observations emphasize the importance of understanding the degradation mechanism of the pure amino acid, L-arginine, as it directly relates to the thermal degradation of the Argopox thermoset. The correlation between the degradation behavior and the amino acid crystals within the thermoset provides valuable insights into the influence of different curing temperatures on the degree of degradation and the resulting properties of the thermoset.

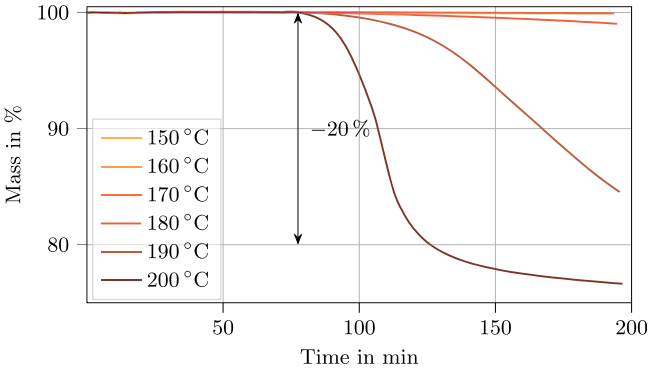

FIGURE 4 Thermo-gravimetric analysis of L-arginine following the curing cycles of Argopox in synthetic air (see Figure 2). [Color figure can be viewed at wileyonlinelibrary.com]

3.3 | Fourier-transform infrared spectroscopy of Argopox

Figure 6 shows the FTIR spectra of Argopox cured at different maximum temperatures T_{max}. The spectra exhibit

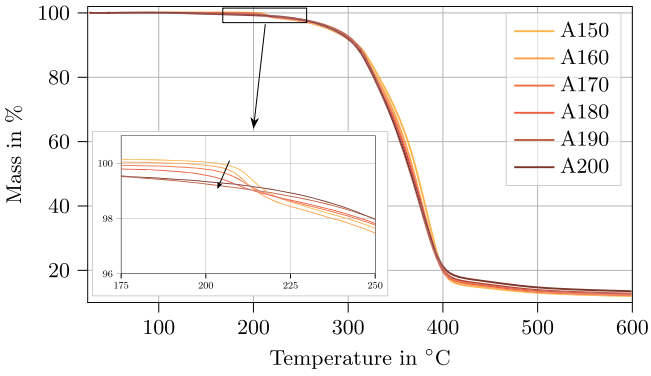

FIGURE 5 Thermo-gravimetric analysis of Argopox cured at different maximum temperatures T_{max}. The close-up shows a detailed view of the degradation at around 210°C. [Color figure can be viewed at wileyonlinelibrary.com]

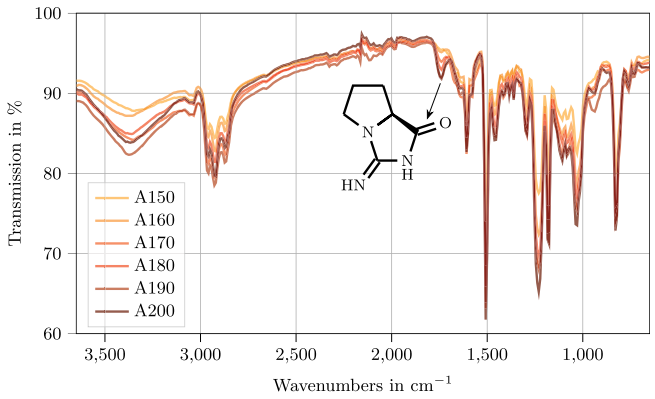

FIGURE 6 FTIR spectra of Argopox cured at different maximum temperatures T_{max}. [Color figure can be viewed at wileyonlinelibrary.com]

peaks that are typical for thermosets consisting of DGEBA resin, such as the H—C═ out-of-plane bending of aromatic rings (825 cm^{-1}), the C—O—C stretching of ether bond (1035 and 1230 cm^{-1}), the C—H in-plane bending (1105 cm^{-1}), the C—O stretching of the aromatic rings (1180 cm^{-1}), the C—C stretching of aromatic rings (1510 cm^{-1}), the C═C stretching of aromatic rings (1610 cm^{-1}) as well as stretching of CH_2 and CH_3 groups (2870 and 2925 and 2960 cm^{-1}) (see Table 2).[45,46] Of course, the urea-based accelerator DYHARD®UR400 also possesses aromatic rings. However, as the weight fraction of the accelerator is much lower than that of the DGEBA resin (see Table 1), the main contribution to the peaks' intensities can be attributed to the epoxy resin.

The presence of peaks corresponding to the guanidino group (1633 and 1673 cm^{-1}) and primary amines (1580, 1610, and 3375 cm^{-1}) in the Fourier-transform infrared spectroscopy (FTIR) analysis of the amino acid side chain indicates the presence of these functional groups in the cured thermoset.

On the other hand, the peaks at 1633 and 1673 cm^{-1} are characteristic of the guanidino group, which constitutes the side chain of L-arginine. These peaks can be attributed to the vibrational modes of the guanidino group, specifically the stretching vibrations of the carbon-nitrogen double bonds within the group.[47,48] The existence of these peaks indicates the presence of the guanidino group in the cured thermoset, specifically in the L-arginine crystals. Similarly, the peaks at 1580, 1610, and 3375 cm^{-1} can be attributed to the vibrations of primary amines present in the amino acid backbone.[49] These peaks correspond to the stretching vibrations of the N—H bonds in the primary amine functional groups.

The sharp peak observed at around 1730–1740 cm^{-1} in the FTIR spectra of the cured Argopox thermosets is indeed indicative of the formation of carbonyl groups. This peak starts to arise from the baseline even at low

TABLE 2 Wavenumbers of characteristic peaks of FTIR spectra of Argopox.

Wavenumbers in cm^{-1}	Band assignment
825	H—C═ out-of-plane bending of aromatic ring
1035	C—O—C stretching of ether linkage
1105	C—H in-plane bending
1180	C—O stretching of aromatic ring
1230	C—O—C stretching of ether linkage
1295	Amide III
1360	CH_2 wagging motion
1385	Symmetrical CH_3 stretching and CH_2 deformation
1412	COO^- symmetrical stretching
1460	CH_2 bending or antisymmetrical CH_3 stretching
1510	C—C stretching of aromatic ring
1580	N—H bending of primary amine
1610	C═C stretching of aromatic ring N—H bending of primary amine
1633	$—CN_3H_5^+$ (guanidino) symmetric stretching
1673	$—CN_3H_5^+$ (guanidino) asymmetric stretching
1740	C═O stretching of β-hydroxy ester or peptide
2100	N—H stretching of amino group in amino acid back bone
2870, 2925, 2960	Stretching vibration of CH_2 and CH_3
3375	O—H stretching and symmetric stretching of primary amine

curing temperatures (150°C), suggesting the formation of β-hydroxy esters through the reaction between the carboxylic acid of the amino acid and the epoxy group of the resin. Similar observations have been reported in studies involving other amino acids, such as L-lysine and L-tryptophan, reacting with epoxy resin.[6,7,10] However, the intensity of this peak increases significantly after curing at temperatures at which thermal degradation of L-arginine occurs (>180°C). This intensified peak is likely attributed to the carbonyl group present in the lactam-like structure of the bicyclic peptide formed during the thermal degradation of L-arginine (see Figure 1).[50] Additionally, the presence of peaks at 1295 (amide III), 1550 (amide II), and 1650 cm^{-1} (amide I) further suggests the formation of peptide bonds and the presence of the resulting bicyclic peptides.[51]

The increase in T_{max} and the corresponding increase in peak intensities in the FTIR spectra are accompanied

by a darkening of the thermosets (see Figure 2, right). Here, the color of the thermosets changes from beige or sand (A150) to yellow-orange (A170) to brown (A190) and, for the highest curing temperature, to dark brown (A200). This darkening is likely associated with the formation of carbonyl groups, which are known to contribute to the browning or darkening of materials under thermal-oxidative stress.[52,53] The significant intensification of the carbonyl peak at 1740 cm^{-1} with increasing curing temperature supports this observation.

3.4 | Differential scanning calorimetry

The DSC analysis presented in Figure 7 (left) provides information about the degree of cure α and glass transition temperature T_g of Argopox cured at different maximum temperatures T_{max}. Starting with A150, the degree of cure is approximately 91%, indicating that the curing process is not yet complete. The corresponding T_g is approximately 87.4°C. Increasing the maximum curing temperature to 160°C results in an increase in both α and T_g by approximately 4% and 7.2°C, respectively. However, even at A160, the thermoset is not fully cured. Further increasing the maximum curing temperature to 170°C leads to almost complete conversion of the epoxy resin (99.7%) and a significant increase in T_g to 104.9°C. At this point, α is nearly 100%, indicating a highly cured thermoset. The increase in T_g is consistent with the high degree of cure achieved.

However, it is worth noting that the increase in T_g becomes less significant when further increasing T_{max}. For instance, the T_g of A180 is 105.6°C, showing only a slight change compared to A170. This suggests that the curing process is already close to completion at 170°C, and higher temperatures have a diminishing effect on T_g. Remarkably, the T_g of A190 and A200 is significantly lower than that of A170 and A180. This indicates that thermo-oxidative aging, occurring during the 2h curing period at temperatures above 190°C, has caused a decrease in the glass transition temperature. Thermo-oxidative aging can lead to the degradation of the polymer network, resulting in changes in its thermal and mechanical properties, including a lower T_g.

Figure 7 (right) presents the DSC thermograms of Argopox thermosets after curing at maximum temperatures T_{max} of 150, 170, and 190°C during the first heating-run. The DSC thermogram of A150 exhibits a glass transition at approximately 87°C. Upon further temperature increase, the curing of the thermoset resumes around 200°C, as evidenced by an exothermic peak. However, this exothermic peak is superimposed by an endothermic peak, which is likely attributed to the thermal degradation of L-arginine crystals. The presence of the endothermic peak suggests that there are L-arginine crystals in the thermoset. The endothermic peak is minimized once T_{max} is increased from 180 to 190°C which is in accordance with the results shown in Figure 4. The effect of the temperature increase on the number of crystals as well as their size and morphology is explained in Section 3.8.

Regarding the heat of reaction, the value obtained in this study (282.6 J g^{-1}) is comparable but slightly lower than the heat of reaction reported by Rothenhäusler et al.[12] Usually, the heat of reaction of solid amine curing agents, such as dicyandiamide, is closer to 350–400 J g^{-1}.[54] The lower heat of reaction observed in the epoxy resin cured with L-arginine, as detected through dynamic DSC measurements, may be attributed to the superposition of the exothermic curing reactions and the endothermic thermal degradation of L-arginine crystals.

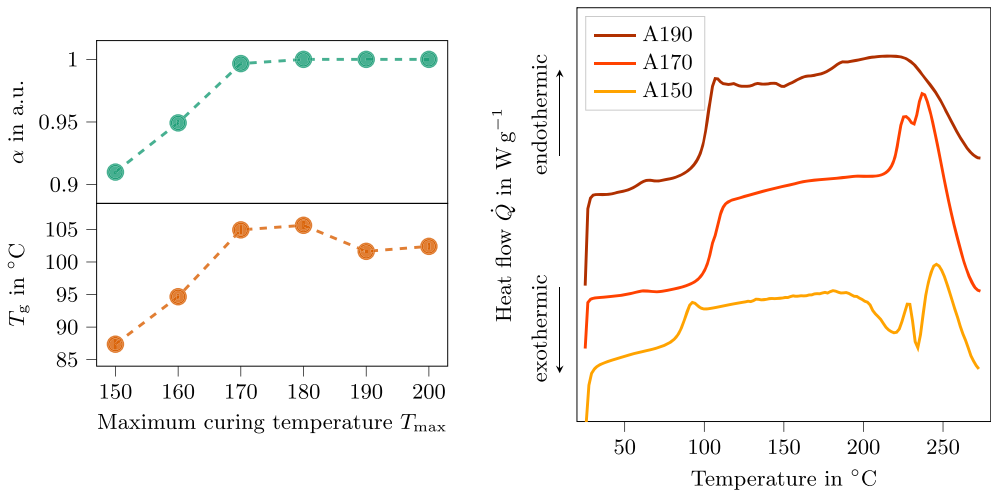

FIGURE 7 Left: Degree of cure α and glass transition temperature T_g of Argopox cured at different maximum temperatures T_{max}. Right: DSC thermograms of the first heating-run of Argopox after curing at maximum temperatures T_{max} of 150, 170, and 190°C. [Color figure can be viewed at wileyonlinelibrary.com]

3.5 | Dynamic mechanical analysis

Figure 8 shows the glass transition temperature T_g, storage modulus E' at $T = 22°C$ and cross-link density ν_C of Argopox cured at different maximum temperatures T_{max}. Similar to the observations in the DSC analysis, an increase in the curing temperature promotes the curing of the thermoset, leading to higher values of ν_C and T_g. It is important to note that determining the absolute value of ν_C in a filled thermoset via DMA is difficult. In this case, L-arginine crystals act as reinforcements in the matrix, thereby increasing the moduli of the thermosets.[33] The changes in ν_C during the curing process of Argopox can be attributed to the increased degree of cure. With a higher degree of cure, the steric hindrance of unreacted amino, carboxyl, and epoxy groups decreases.[18,19] As a result, the storage modulus E' decreases with higher T_{max}. Above 180°C, the decrease in E' can be attributed to the thermal degradation of L-arginine crystals, as discussed in the SEM analysis (see Section 3.8). As a result of thermal degradation, the L-arginine crystals undergo chemical changes, thereby losing mass and volume. The adhesion between the amino acid crystals and the surrounding matrix is diminished. As a result, the load-bearing cross-section of the DMA specimens is reduced significantly. Additionally, the total volume of reinforcing crystals is reduced. Both effects contribute to the decrease in E'.

In comparison to a previous study on L-arginine as a curing agent, the cross-link density ν_C obtained in this study is considerably lower than that of the thermoset cured with DYHARD®UR500 as an accelerator (2540 mol m^{-3}). However, the T_g and E' values of both thermosets are similar.[13]

3.6 | Three-point bending

Figure 8 illustrates the flexural modulus E_F, flexural strength σ_F and fracture strain ε_F of Argopox cured at different maximum temperatures T_{max}. The flexural modulus shows a continuous decrease with increasing T_{max} from 3.4 GPa for A150 to 3.1 GPa for A180. However, there is a subsequent increase in modulus to 3.4 GPa for A190, followed by a decrease to 3.2 GPa for A200. However, there is no explanation for the increase in modulus at 190°C.

In contrast, the flexural strength increases from approximately 97 MPa for A150 to around 109 MPa for A170. For higher maximum curing temperatures, the strength decreases again, with a significant drop from 102 MPa for A190 to 82 MPa for A200. The higher cross-link density resulting from increased curing temperatures contributes to the higher flexural strength. However, as the thermoset becomes more brittle, it becomes more susceptible to failure due to defects such as voids or cracks. Specifically, in the case of epoxy resins cured with amino acid, the thermal degradation of the amino acid crystals diminishes the adhesion between the THL-arginine crystals and the epoxy matrix. As a result, the L-arginine crystals, which would typically act as reinforcements, now constitute defects within the matrix. This effect of the degradation of L-arginine crystals on the flexural strength is consistent with the higher standard deviation observed for A200, indicating a greater variability in strength due to the presence of defects caused by the degradation of L-arginine crystals at elevated temperatures, as discussed in Section 3.8. Similarly, the flexural strain at failure follows a similar trend, reaching its maximum at $T_{max} = 170°C$ and decreasing for higher curing temperatures. The higher

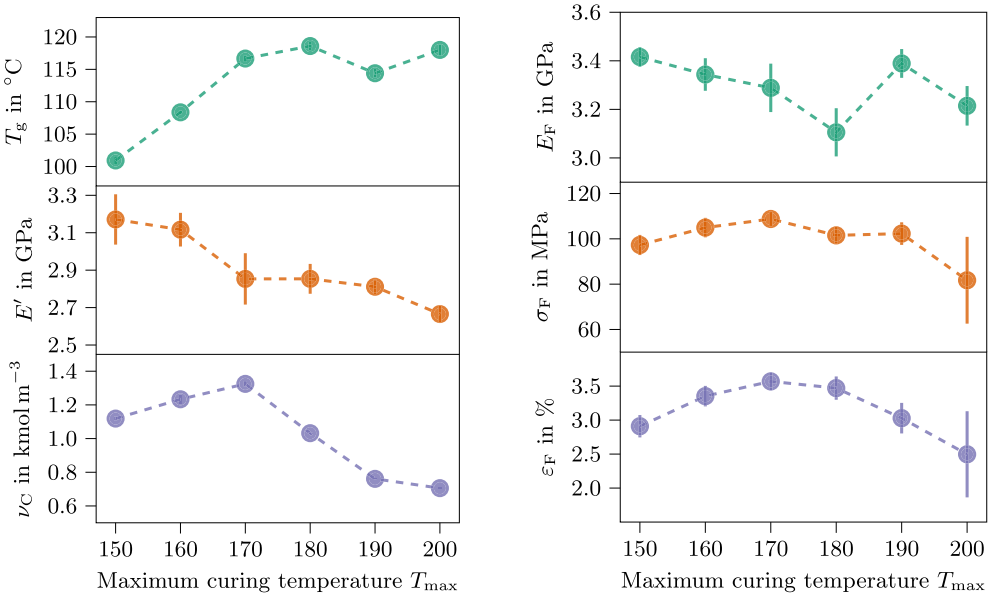

FIGURE 8 Left: Glass transition temperature T_g, storage modulus E' at $T = 22°C$ and cross-link density ν_C of Argopox cured at different maximum temperatures T_{max} according to DMA. Right: Flexural modulus E_F, flexural strength σ_F and fracture strain ε_F of Argopox cured at different maximum temperatures T_{max} according to three-point bending tests. [Color figure can be viewed at wileyonlinelibrary.com]

cross-link density ν_C limits the extent of deformation the thermosets can undergo before failure.

The flexural strength of A170 is comparable to DGEBA cured with conventional, petroleum-based amine curing agents (95–123 MPa).[55] In another study by Rothenhäusler et al.,[13] the flexural properties of DGEBA cured with L-arginine were characterized. However, the flexural modulus and strength were considerably lower than the results of this study. In that study, the modulus and strength at room temperature were 2.9 GPa and 85 MPa, respectively. Therefore, the different curing cycles and accelerators used have a significant influence on the flexural properties of DGEBA cured with L-arginine.

3.7 | Fracture toughness

Figure 9 shows the critical stress intensity factor in mode I K_{IC} and fracture energy G_{IC} of Argopox cured at different maximum temperatures T_{max}. Here, K_{IC} decreases continuously from 1.19 MPa m$^{0.5}$ for A150 to 0.91 MPa m$^{0.5}$ for A190, followed by a sudden drop to 0.6 MPa m$^{0.5}$ for A200. Similarly, G_{IC} decreases from 366 J m^{-2} for A150 to 102 J m^{-2} for A200. The increase in degree of cure leads to an increase in cross-link density, making the thermoset more brittle.[20] The sudden drop in fracture toughness from A190 to A200 is most likely caused by the degradation of L-arginine crystals (see Section 3.8). The adhesion between the amino acid crystals and the epoxy matrix is diminished. As a result, the degraded crystals act as defects, leading to high stress concentrations around them.

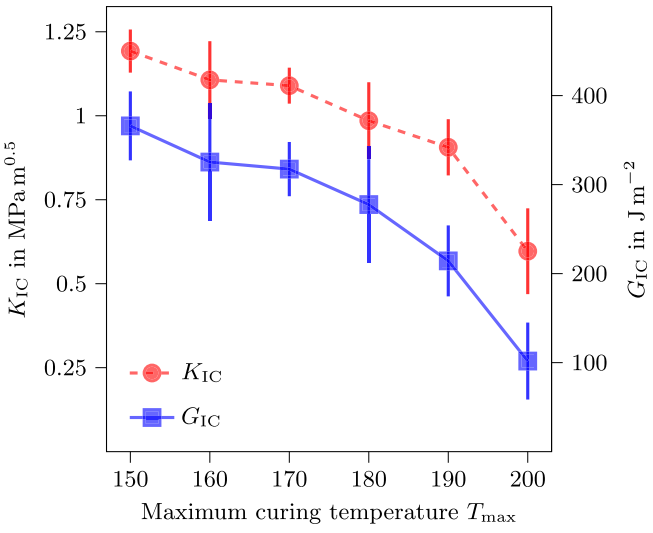

FIGURE 9 Critical stress intensity factor in mode I K_{IC} and fracture energy G_{IC} of Argopox cured at different maximum temperatures T_{max}. [Color figure can be viewed at wileyonlinelibrary.com]

The critical stress intensity factor K_{IC} of unfilled epoxides usually ranges from 0.6 to 0.7 MPa m$^{0.5}$.[56–58] After the observation of amino acid crystal formation in epoxides (see Reference 33), it can be concluded that the increased fracture toughness is the result of the toughening effect of L-arginine crystals in the epoxy matrix.

Comparing the results to previous investigations, the fracture toughness of A170 (1.09 MPa m$^{0.5}$) aligns well with the fracture toughness of DGEBA cured with L-arginine in the presence of another urea-based accelerator (1.09 MPa m$^{0.5}$).[13] This suggests that the different structures of the urea-based accelerators did not have a significant influence on the fracture toughness of the thermosets.

3.8 | Scanning electron microscopy

Figure 10 shows the scanning electron microscopy images of A150 at different magnifications. Figure 10a gives an overview about the rough fracture surface with numerous inclusions with different particle sizes. Similar to the observations by Rothenhäusler et al.[33] in a study about the mechanical properties of DGEBA cured with L-tyrosine, it can be assumed that the particles are L-arginine crystals. Figure 10b shows the fracture surface and the crystals in more detail. Here, in left section of the figure, it can be observed that the crystal was broken during the compact tension test which indicates that the crystal is well bonded to the surrounding thermoset matrix. In contrast to the rod-like crystals of L-tyrosine,[33] the L-arginine crystals appear to be closer to spherical particles. However, determining the exact shape of the crystals is hardly possible as they are broken and partially covered with matrix. Vickery et al.[59] described L-arginine crystals as rectangular prisms which roughly fits the description of the particles depicted in Figure 10c. Here, the fracture surface shows distinctive fracture patterns and crystals with sizes between 20 and 30 µm. The presence of characteristic lines formed during crack propagation suggests the activation of toughening mechanisms such as crack pinning, crack deflection, and crack bifurcation.[60,61] Next, Figure 10d shows L-arginine crystals with sizes below 1 µm. Furthermore, the fracture surface is, even on a nano-meter length scale, not smooth. This contributes to the thermosets' high fracture toughness.

Figure 11 shows scanning electron microscopy images of fracture surfaces of compact tension specimens made from Argopox cured at different maximum curing temperatures at 500× magnification. A comparison between Figure 11b,c reveals that higher curing temperatures

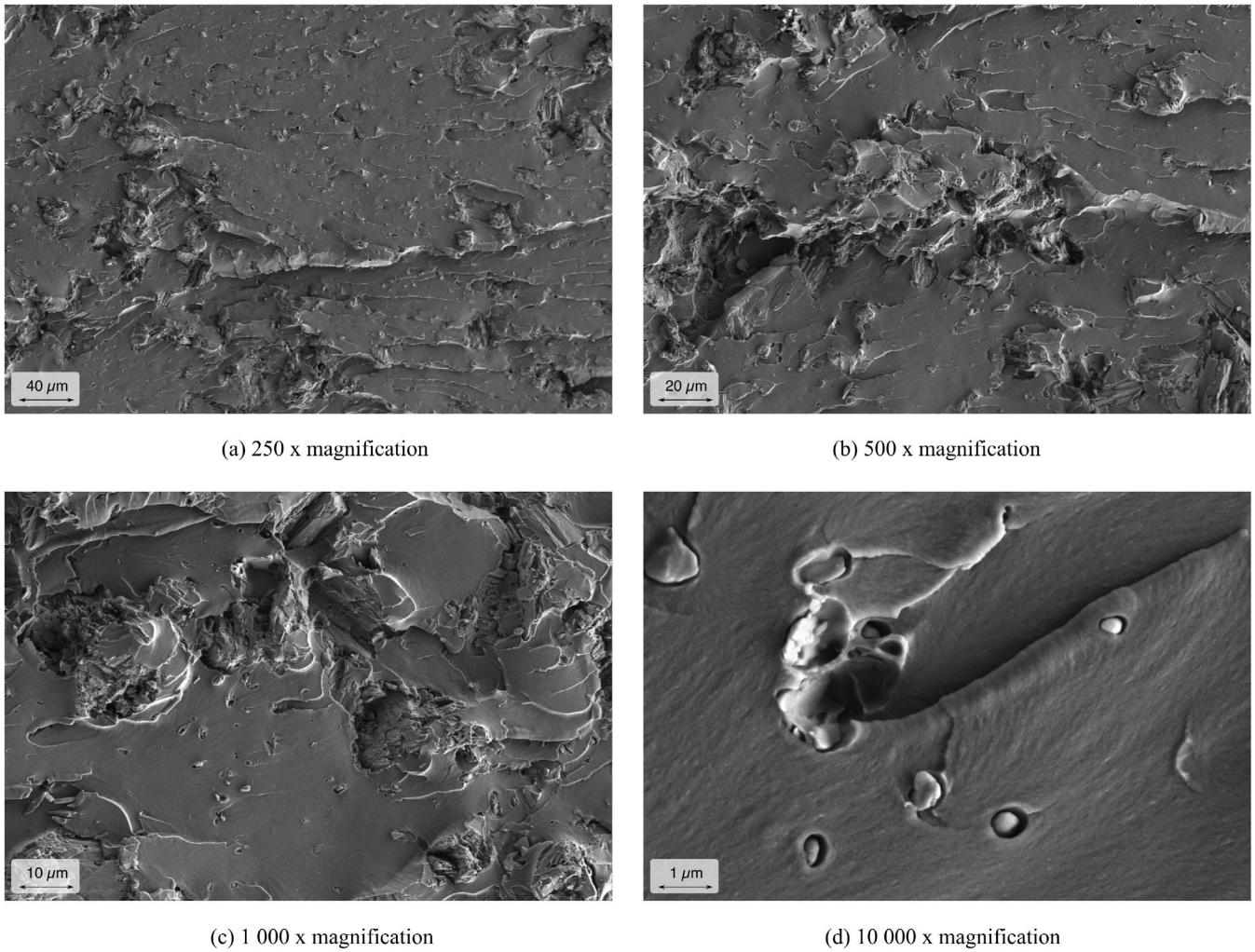

(a) 250 x magnification

(b) 500 x magnification

(c) 1 000 x magnification

(d) 10 000 x magnification

FIGURE 10 Fracture surfaces of compact tension specimens made from A150 at 250× (a), 500× (b), 1000× (c), and 10,000× magnification (d).

result in a smoother fracture surface. As discussed in the previous sections, increased curing temperatures facilitate the rearrangement of network segments and increase the degree of cure. Consequently, the cross-link density increases, making the thermosets more brittle. This trend continues for A180. However, a further increase in curing temperature has a significant impact on the fracture surface topology, as well as on the number and morphology of L-arginine crystals.

Figure 11e shows that the abundance of smaller crystals with a size of 1 μm disappears, leaving voids in the fracture surface. Moreover, the larger crystals are significantly smaller compared to those observed in Figure 11d. The crystals become more spherical due to the temperature increase, and particle pull-out during fracture propagation leads to round holes in the fracture surface. The spherical crystals are also less covered with thermoset matrix, indicating a diminished crystal-matrix adhesion caused by the temperature increase and subsequent thermal degradation of L-arginine crystals. These observations become even more pronounced for A200 (see Figure 11f). The spherical crystals now act as defects in the matrix which explains the significant loss in storage modulus, flexural strength and fracture toughness. In conclusion, curing regimes that include temperatures above 180°C degrade the L-arginine crystals and cause significant changes in mechanical properties.

3.9 | Structure–property relationships

Lastly, structure–property relationships are derived by correlating the results of DSC, DMA, three-point bending and compact tension tests at maximum curing temperatures of T_{max} = 150, 160, and 170°C. The Pearson product–moment correlation coefficients R_P[62] (see Figure 12) were calculated via *numpy.corrcoef()* in Python 3.8.0[63] to assess the correlations between the maximum curing

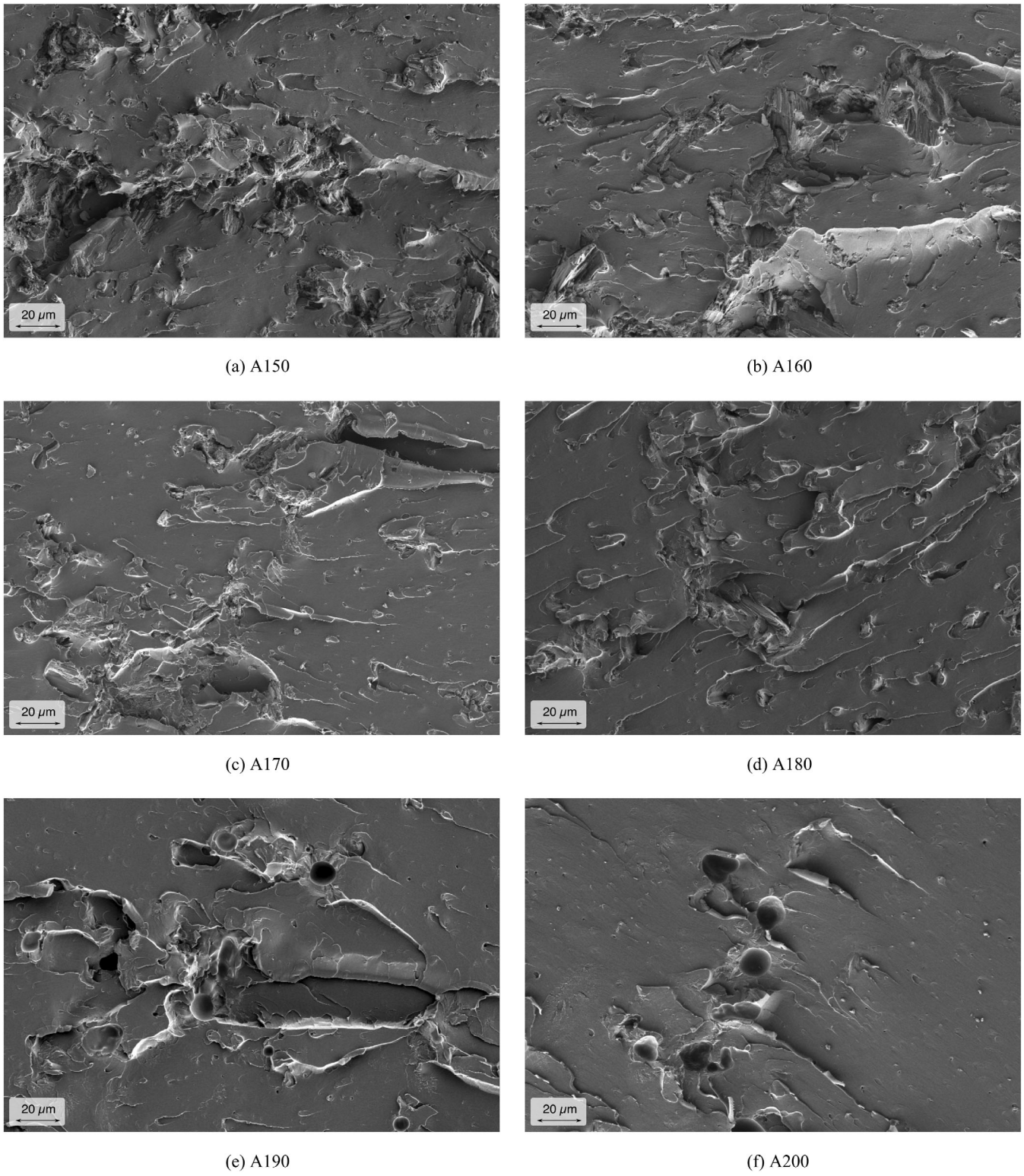

(a) A150 (b) A160

(c) A170 (d) A180

(e) A190 (f) A200

FIGURE 11 Fracture surfaces of compact tension specimens made from Argopox cured at different maximum curing temperatures at 500× magnification.

temperature T_{max}, degree of cure α, glass transition temperature T_g, cross-link density ν_C, flexural modulus E_F, flexural strength σ_F, critical stress intensity factor in mode I K_{IC} and fracture energy G_{IC} of Argopox cured at $T = 150$, 160, and 170°C. Since the degree of cure is constant for temperatures above 170°C and thus the R_P from it cannot be calculated, only the results of Argopox cured between 150 and 170°C could be used.

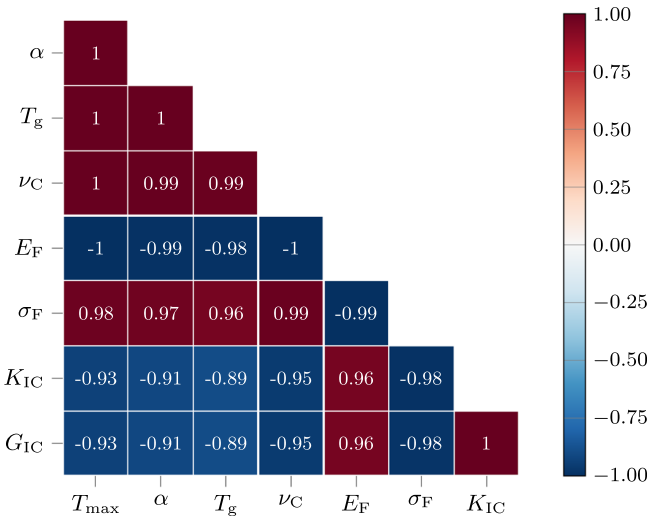

FIGURE 12 Pearson product–moment correlation coefficients R_P of the maximum curing temperature T_{max}, degree of cure α, glass transition temperature T_g, cross-link density ν_C, flexural modulus E_F, flexural strength σ_F, critical stress intensity factor in mode I K_{IC} and fracture energy G_{IC} of Argopox cured at $T = 150$, 160, and 170°C. [Color figure can be viewed at wileyonlinelibrary.com]

The maximum curing temperature T_{max} has a positive correlation with the degree of cure α ($R_P = 1$), indicating that higher temperatures increase the mobility within the thermoset network.[17] This enhanced mobility facilitates the rearrangement of network segments and promotes the reaction between unreacted functional groups of DGEBA and L-arginine, leading to an increase in α and the cross-link density ν_C ($R_P = 1$). Additionally, the stiffer network resulting from a higher T_{max} leads to an increase in the glass transition temperature T_g ($R_P = 0.99$).[64,65]

The degree of cure α and the maximum curing temperature T_{max} are positively correlated. The steric hindrance of unreacted functional groups in DGEBA and L-arginine decreases as the temperature increases, resulting in a decrease in the flexural modulus E_F ($R_P = -1$).[66,67] The higher cross-link density ν_C obtained at higher temperatures contributes to an increase in the flexural strength σ_F ($R_P = 0.99$).

On the other hand, an increased cross-link density ν_C leads to thermoset embrittlement ($R_P = -0.95$).[20,68,69] Consequently, the critical stress intensity factor K_{IC} and fracture energy G_{IC} decrease with higher T_{max} ($R_P = -0.93$). As mentioned in a previous study,[14] depending on the network density, thermosets can exhibit high strength or high toughness but rarely both simultaneously. Moreover, a perfect correlation ($R_P = 1$) was observed between K_{IC} and G_{IC} since G_{IC} is calculated based on K_{IC}.[70] Materials with high resistance to unstable crack propagation tend to dissipate more energy during crack propagation.

4 | CONCLUSION AND OUTLOOK

The present study aimed to investigate the impact of maximum curing temperature on the network structure, crystal morphology, and mechanical properties of DGEBA cured with L-arginine in order to determine an optimal curing cycle. The maximum curing temperature can be divided into two distinct regimes. The first regime encompasses the temperature range at which the thermoset achieves complete curing without causing thermal degradation of the amino acid crystals. This regime extends up to 170°C for a duration of 2 h. The second regime begins when the thermoset is fully cured and the thermal degradation starts to adversely affect its mechanical properties. This degradation is observed to commence at a minimum of 180°C for 2 h. During their thermal degradation, the L-arginine crystals release ammonia and water. Consequently, the amino acid crystals undergo chemical changes, as well as changes in crystal size and crystal morphology. As a result, the adhesion between amino acid crystals and the surrounding epoxy matrix is lowered substantially. The close proximity of these temperature ranges, even for short periods, can be attributed to the low thermal stability of the aliphatic amino acid, L-arginine, and the low reactivity of the resin system.

The derived structure–property relationships highlight the significance of carefully designing the curing cycles to achieve specific mechanical performance requirements. For instance, a favorable curing cycle for achieving high flexural strength and adequate fracture toughness may involve an initial period of 1 h at 150°C followed by 2 h at 170°C. The correlation between the degradation behavior of the amino acid crystals within the thermoset and the resulting mechanical properties provides valuable insights into the influence of different curing temperatures on the overall mechanical performance of the thermoset.

Furthermore, it is important to consider other potential regimes beyond the two discussed above. The presence of various factors such as the accelerator's ability to lower the activation energy for the curing reaction, the reactivities of the epoxy resin and the amino acid, and the thermal stability of the amino acid can result in different scenarios. These scenarios include: (1) the thermoset curing without any degradation of the amino acid, (2) the possibility of further temperature increase without causing thermal degradation of the amino acid, and (3) the amino acid degrading before or during the completion of thermoset curing.

AUTHOR CONTRIBUTIONS

Florian Rothenhäusler: Conceptualization (lead); data curation (lead); formal analysis (lead); investigation (lead); methodology (lead); validation (lead); visualization (lead); writing – original draft (lead). **Holger Ruckdaeschel:** Project administration (lead); resources (lead); supervision (lead); writing – review and editing (lead).

ACKNOWLEDGMENTS

The authors want to thank Gokul Varadharajan, Ute Kuhn, and Annika Pfaffenberger for their support during the experiments. We would like to thank all colleagues of the work group "Resins & Composites" at the Department of Polymer Engineering for their support. Open Access funding enabled and organized by Projekt DEAL.

FUNDING INFORMATION

Parts of the research documented in this manuscript have been funded by the German Federal Ministry for Economic Affairs and Climate Action (BMWK) within the research project "EcoPrepregs—Grundlagenforschung zur Klärung der Struktur-Eigenschaftsbeziehungen von Epoxidharzen und Fasern aus nachwachsenden Rohstoffen zur Anwendung in der Sekundärstruktur von Flugzeugen" (grant # 20E1907A, Germany).

CONFLICT OF INTEREST STATEMENT

There are no conflicts of interest associated with this publication.

DATA AVAILABILITY STATEMENT

The data that support the findings of this study are available from the corresponding author upon reasonable request.

ORCID

Florian Rothenhäusler https://orcid.org/0000-0001-9948-3310

Holger Ruckdaeschel https://orcid.org/0000-0001-5985-2628

REFERENCES

[1] H. Schürmann, *Konstruieren mit Faser-Kunststoff-Verbunden*, Springer, Berlin **2007**.
[2] G. W. Ehrenstein, *Faserverbund-Kunststoffe*, Carl Hanser Verlag GmbH & Co. KG, Munich **2006**.
[3] H. Lengsfeld, F. Wolff-Fabris, J. Krämer, J. Lacalle, V. Altstädt, *Faserverbundwerkstoffe – Prepregs und ihre Verarbeitung*, Hanser Publishers, Munich **2014**.
[4] S. Kumar, S. Samal, S. Mohanty, S. Nayak, *Polym.-Plast. Technol. Eng.* **2016**, *12*, 57.
[5] A. Gholampour, T. Ozbakkaloglu, *J. Mater. Sci.* **2020**, *55*, 829.
[6] Y. Li, F. Xiao, K. Moon, C. P. Wong, *J. Polym. Sci., Part A: Polym. Chem.* **2005**, *44*, 1020.
[7] Y. Li, F. Xiao, C. P. Wong, *J. Polym. Sci., Part A: Polym. Chem.* **2007**, *45*, 181.
[8] A. Motahari, A. Omrani, A. A. Rostami, *Comput. Theor. Chem.* **2011**, *977*, 168.
[9] L. Mazzocchetti, S. Merighi, T. Benelli, L. Giorgini, *AIP Conf. Proc.* **2018**, *1981*, 020170.
[10] M. Shibata, J. Fujigasaki, M. Enjoji, A. Shibita, N. Teramoto, S. Ifuku, *Eur. Polym. J.* **2018**, *98*, 216.
[11] S. Merighi, L. Mazzocchetti, T. Benelli, L. Giorgini, *Processes* **2021**, *9*, 42.
[12] F. Rothenhäusler, H. Ruckdaeschel, *Polymer* **2022**, *14*, 4331.
[13] F. Rothenhäusler, H. Ruckdaeschel, *Polymer* **2022**, *14*, 4696.
[14] F. Rothenhäusler, H. Ruckdaeschel, *Polymer* **2023**, *15*, 385.
[15] J. K. Gillham, in *The Time-Temperature-Transformation (TTT) State Diagram and Cure Boston* (Eds: J. C. Seferis, L. Nicolais), Springer US, MA **1983**, p. 127.
[16] S. L. Simon, J. K. Gillham, *J. Appl. Polym. Sci.* **1994**, *53*, 709.
[17] M. Wolfahrt, *PhD Thesis*, Montanuniversität Leoben **2009**.
[18] C. H. Lau, K. A. Hodd, W. W. Wright, *Brit. Polym. J.* **1986**, *18*, 316.
[19] J. P. Pascault, R. J. J. Williams, *J. Polym. Sci., Part B: Polym. Phys.* **1990**, *28*, 85.
[20] G. Levita, S. De Petris, A. Marchetti, A. Lazzeri, *J. Mater. Sci.* **1991**, *26*, 2348.
[21] E. Espuche, J. Galy, J. F. Gérard, J. P. Pascault, H. Sautereau, *Macromol. Symp.* **1995**, *93*, 107.
[22] Y. Pei, K. Wang, M. Zhan, W. Xu, X. Ding, *Polym. Degrad. Stab.* **2011**, *96*, 1179.
[23] I. M. Hodge, *Science* **1995**, *267*, 1945.
[24] S. L. Maddox, J. K. Gillham, *J. Appl. Polym. Sci.* **1997**, *64*, 55.
[25] L. Barral, J. Cano, J. López, I. López-Bueno, P. Nogueira, M. J. Abad, C. Ramírez, *J. Therm. Anal. Calorim.* **2000**, *60*, 391.
[26] L. Barral, J. Cano, J. López, P. Nogueira, C. Ramírez, *J. Appl. Polym. Sci.* **1997**, *63*, 1841.
[27] J. Decelle, N. Huet, V. Bellenger, *Polym. Degrad. Stab.* **2003**, *81*, 239.
[28] C. Bockenheimer, D. Fata, W. Possart, *J. Appl. Polym. Sci.* **2004**, *91*, 361.
[29] B. Mailhot, S. Morlat-Thérias, M. Ouahioune, J. L. Gardette, *Macromol. Chem. Phys.* **2005**, *206*, 575.
[30] P. G. Olafsson, A. M. Bryan, *Microchim. Acta* **1970**, *58*, 871.
[31] G. Chiavari, G. C. Galletti, *J. Anal. Appl. Pyrolysis* **1992**, *24*, 123.
[32] F. Rodante, G. Marrosu, G. Catalani, *Thermochim. Acta* **1992**, *194*, 197.
[33] F. Rothenhäusler, H. Ruckdaeschel, *Polym. Eng. Sci.*
[34] M. Neĭman, B. Kovarskaya, L. Golubenkova, A. Strizhkova, I. Levantovskaya, M. Akutin, *J. Polym. Sci.* **2003**, *3*, 383.
[35] D. Bishop, D. Smith, *Ind. Eng. Chem.* **1967**, *59*, 32.
[36] I. M. Weiss, C. Muth, R. Drumm, H. O. K. Kirchner, *BMC Biophys.* **2018**, *11*, 2.
[37] L. Jie, L. Yuwen, S. Jingyan, W. Zhiyong, H. Ling, Y. Xi, W. Cunxin, *Thermochim. Acta* **2008**, *467*, 20.
[38] W. Ji, B. Xue, Z. A. Arnon, H. Yuan, S. Bera, Q. Li, D. Zaguri, N. P. Reynolds, H. Li, Y. Chen, S. Gilead, S. Rencus-Lazar, J. Li, R. Yang, Y. Cao, E. Gazit, *ACS Nano* **2019**, *13*, 14477.
[39] A. Greenberg, C. M. Breneman, J. F. Liebman, *The Amide Linkage: Structural Significance in Chemistry, Biochemistry, and Materials Science*, John Wiley & Sons, Hoboken, New Jersey **2000**.

[40] A. B. Hughes, *Amino Acids, Peptides and Proteins in Organic Chemistry, Analysis and Function of Amino Acids and Peptides*, John Wiley & Sons, Hoboken, New Jersey **2013**.
[41] Q. Albuquerque, F. Rothenhäusler, H. Ruckdaeschel, *MRS Bull.* **2023**, *48*, 1.
[42] X. Y. Zhao, W. Jiang, Y. F. Shan, J. P. Cao, *Energy Fuels* **2022**, *36*, 502.
[43] G. Laroche, J. Vallade, R. Bazinette, P. Van Nijnatten, E. Hernandez, G. Hernandez, F. Massines, *Rev. Sci. Instrum.* **2012**, *10*, 103508.
[44] M. Palencia, *J. Adv. Res.* **2018**, *5*, 14.
[45] A. Cherdoud-Chihani, M. Mouzali, M. J. M. Abadie, *J. Appl. Polym. Sci.* **2003**, *87*, 2033.
[46] C. A. Ramírez-Herrera, I. Cruz-Cruz, I. H. Jiménez-Cedeño, O. Martínez-Romero, A. Elías-Zúñiga, *Polymer* **2021**, *13*, 1273.
[47] R. J. Koegel, J. P. Greenstein, M. Winitz, S. M. Birnbaum, R. A. McCallum, *J. Am. Chem. Soc.* **1955**, *77*, 5708.
[48] S. Y. Venyaminov, N. N. Kalnin, *Biopolymers* **1990**, *30*, 1243.
[49] H. Günzler, H. U. Gremlich, *IR Spectroscopy*, Wiley-VCH, Weinheim **2002**.
[50] M. Gil, J. L. Núñez, M. A. Palafox, N. Iza, *Biopolymers* **2001**, *62*, 278.
[51] S. Y. Venyaminov, N. N. Kalnin, *Biopolymers* **1990**, *30*, 1259.
[52] A. E. Krauklis, A. T. Echtermeyer, *Polymers* **2018**, *10*, 10.
[53] C. Wu, B. C. Meng, L. ho Tam, L. He, *Polym. Test.* **2022**, *114*, 107708.
[54] M. D. Gilbert, *Mechanism and kinetics of the dicyandiamide cure of epoxy resins* **1988**.
[55] F. G. Garcia, B. G. Soares, V. J. R. R. Pita, R. Sánchez, J. Rieumont, *J. Appl. Polym. Sci.* **2007**, *106*, 2047.
[56] R. J. Varley, *Polym. Int.* **2004**, *53*, 78.
[57] B. C. Kim, S. W. Park, D. G. Lee, *Compos. Struct.* **2008**, *86*, 69.
[58] F. Hübner, M. Hoffmann, N. Sommer, V. Altstädt, A. Scherer, T. Dickhut, H. Ruckdäschel, *Polym. Test.* **2022**, *113*, 107678.
[59] H. B. Vickery, C. S. Leavenworth, *J. Biol. Chem.* **1928**, *76*, 701.
[60] B. Wetzel, P. Rosso, F. Haupert, K. Friedrich, *Eng. Fract. Mech.* **2006**, *73*, 2375.
[61] A. Zotti, S. Zuppolini, M. Zarrelli, A. Borriello, *Fracture Toughening Mechanisms in Epoxy Adhesives* **2016**.
[62] A. Bravais, *Analyse mathématique sur les probabilités des erreurs de situation d'un point*, Impr. Royale, Paris **1844**.
[63] NumPy-Developers, numpy.corrcoef()-function **2023**. https://numpy.org/doc/stable/reference/generated/numpy.corrcoef.html
[64] T. D. Chang, S. H. Carr, J. O. Brittain, *Polym. Eng. Sci.* **1982**, *22*, 1213.
[65] M. Shimbo, N. Nishitani, T. Takahama, *J. Appl. Polym. Sci.* **1984**, *29*, 1709.
[66] V. B. Gupta, L. T. Drzal, C. Y. C. Lee, M. J. Rich, *Polym. Eng. Sci.* **1985**, *25*, 812.
[67] F. Meyer, G. Sanz, A. Eceiza, I. Mondragon, J. Mijović, *Polymer* **1995**, *36*, 1407.
[68] H. Kishi, T. Naitou, S. Matsuda, A. Murakami, Y. Muraji, Y. Nakagawa, *J. Polym. Sci., Part B: Polym. Phys.* **2007**, *45*, 1425.
[69] R. Rahul, R. Kitey, *Composites, Part B* **2016**, *85*, 336.
[70] G. R. Irwin, *J. Appl. Mech.* **1957**, *24*, 361.

How to cite this article: F. Rothenhäusler, H. Ruckdaeschel, *J. Appl. Polym. Sci.* **2023**, *140*(45), e54655. https://doi.org/10.1002/app.54655